

THE GAS DYNAMICS OF H II REGIONS. II. TWO-DIMENSIONAL AXISYMMETRIC CALCULATIONS¹

P. BODENHEIMER, G. TENORIO-TAGLE, AND H. W. YORKE

Max-Planck-Institut für Physik und Astrophysik

Received 1978 November 28; accepted 1979 April 3

ABSTRACT

The evolution of H II regions is calculated with a two-dimensional hydrodynamic numerical procedure under the assumption that the exciting star is born within a cool molecular cloud whose density is about 10^3 particles cm^{-3} . As the ionization of the cloud's edge is completed, a large pressure gradient is set up and ionized cloud material expands into the ionized low-density (1 particle cm^{-3}) intercloud medium, with velocities larger than 30 km s^{-1} .

The calculations are made under the simplifying assumptions that (i) within the H II region, ionization equilibrium holds at all times, (ii) the ionization front is a discontinuity, thus its detailed structure is not calculated, (iii) the temperature of each region (H II region, neutral cloud, and intercloud medium) is constant in time, (iv) all ionizing photons come radially from the exciting star. Four cases are calculated and compared with observations: (1) the edge of the cloud is overrun by a supersonic ionization front, (2) the initial Strömgren sphere surrounding the star lies deep inside the cloud, thus the cloud's edge is ionized by a subsonic ionization front, (3) the ionization front breaks through two opposite faces of the same cloud simultaneously, (4) the flow encounters an isolated globule of density 10^3 particles cm^{-3} shortly after emerging from the molecular cloud.

The phenomena here considered show how evolving H II regions are an important input of kinetic energy to the interstellar medium.

Subject headings: hydrodynamics — nebulae: general

I. INTRODUCTION

Previous studies of the evolution of H II regions have shown three well-defined phases. These have been worked out with a variety of analytical and numerical techniques (for comprehensive reviews see Mathews and O'Dell 1969 and Terzian and Balick 1974), in most cases under the assumption that an early-type star is embedded in a medium of constant density n_0 atoms cm^{-3} . During the formation phase (as the star moves onto the main sequence) the large supply of photons produces a supersonic ionization front. This front slows down as it approaches the Strömgren radius [$R_s = (3F_*/4\pi\beta n_0^2)^{1/3}$, where F_* is the total number of photons s^{-1} produced by the star and β is the recombination coefficient] and eventually develops a shock wave which moves ahead of it into the surrounding gas as the H II region begins to expand.

During the expansion phase the ionization front is always of the *D*-type, and rarefaction waves move toward the central source, causing a decrease in the number of recombinations in the H II region. This enables the ionization front to constantly sweep up new material. Nevertheless, most of the gas swept up by the leading shock remains neutral and forms a cool dense shell between the two fronts. This phase comes to an end when the pressure of the rarefied H II region becomes comparable to the pressure of the undisturbed surrounding gas. A final phase of the evolution occurs

when the exciting star moves off the main sequence and the H II region recombines and cools. Mansfield (1972) has shown the main characteristics of the remnant which make its identification unambiguous.

Although the evolution of an H II region (for the constant-density case) is well understood theoretically, the model has failed to explain many observational facts (for a summary of these, see Osterbrock 1974). It has been shown, however (Tenorio-Tagle 1979, hereafter Paper I), that the agreement between the model and the observations can be improved if one considers a solution to the problem (obtained with different initial conditions) that introduces a new evolutionary phase. Based on the observed physical association that exists between all H II regions and dense clouds, and the fact that star formation is more likely to occur inside the clouds, he performed a series of time-dependent calculations assuming plane symmetry and a cloud of density n_c ($n_c = 100, 500, \text{ and } 10^3 \text{ cm}^{-3}$) in which an early-type star has formed. The calculations allowed the H II region to encounter the density discontinuity between cloud and intercloud (IC) media at various stages of its evolution. The solutions showed how the ionization front (*I* front) in all cases becomes supersonic after crossing the discontinuity, causing a large pressure gradient between the ionized cloud and IC media. The pressure discontinuity produces a "champagne effect" by resolving itself into a strong isothermal shock (Mach $\gtrsim 3$) moving into the ionized IC medium and a rarefaction wave traveling toward

¹ *Lick Observatory Bulletin*, No. 830.

the star. As the ionized cloud becomes rarefied, its material streams with supersonic velocities away from the cloud and diffuses over a very large radius. In this way many observations (e.g., the run of density and velocity along different lines of sight, the broadened emission lines in H α , [O III], etc.) can now be explained.

An H II region will undergo the phase described above as soon as its outward facing *I* front ionizes the cloud-IC discontinuity. Before that, the nebula is ionization bounded, and it might be detectable only in the radio continuum. During this stage, the "classical" theory will describe accurately enough its evolution. Once the champagne phase begins, the ionized material swept up by the isothermal shock might be observationally identified as the edge of the extended nebula since the emission produced by the outer ionized unshocked IC gas is negligible. Thus, this side of the nebula becomes density bounded.

In the present paper we extend the hydrodynamic numerical calculations of the evolution of H II regions in dense clouds to two space dimensions with axial symmetry and are thus able to treat geometrical situations that cannot be solved using plane-parallel or spherical symmetry. The specific problems treated emphasize the behavior of flows that cross a discontinuity between a cloud and the low-density IC medium. Our calculations are approximate in the sense that the numerical resolution is not as good as that generally employed in one-dimensional (1-D) solutions, so that the detailed structure of ionization fronts and shock fronts is not calculated. Nevertheless, the solutions should produce the correct overall flow patterns and fluid velocities, and therefore can be considered as a useful guide to the general types of evolution expected in an ionized nebula. In § II we outline the approximations and procedures that are employed, in § III we present results for four particular cases, and in § IV we discuss the results and compare them with some well-known observed examples.

II. METHOD AND APPROXIMATIONS

The equations of hydrodynamics are expressed in cylindrical coordinates (X, Z, ϕ) with symmetry axis Z and with derivatives in ϕ suppressed. They are solved on a two-dimensional 40×40 (X, Z) numerical grid that remains fixed in space. If ρ is the gas density, P the gas pressure, v the gas velocity, and I, J , respectively, the linear momenta per unit volume in the X - and Z -directions, then the equations can be expressed as follows:

$$\frac{\partial \rho}{\partial t} + \nabla \cdot (\rho v) = 0, \quad (1)$$

$$\frac{\partial I}{\partial t} + \nabla \cdot (Iv) = -\frac{\partial P}{\partial X}, \quad (2)$$

$$\frac{\partial J}{\partial t} + \nabla \cdot (Jv) = -\frac{\partial P}{\partial Z}. \quad (3)$$

They are supplemented by conditions on the gas temperature, discussed below, and by the ideal-gas

equation of state for a pure hydrogen gas. There are no motions in the ϕ -direction, and the self-gravity of the cloud is not considered in the present paper.

The solution to the equations is carried out by an explicit numerical technique discussed in detail by Black and Bodenheimer (1975); the grid motion described in that paper is, however, not included. The outer boundary of the grid is in general taken to be a free surface across which material is allowed to flow. No special provisions are made for the treatment of shock fronts. The numerical viscosity that appears in regions with steep density gradients is sufficient to smooth shocks over two or three zones.

To solve the hydrodynamic equations (1)–(3) it is necessary to calculate the ratio T/μ of the temperature and the mean molecular weight of the gas at each point in space. In principle this quantity is obtained through a detailed solution of the equation of conservation of energy, including heating and cooling mechanisms, along with the coupled equations for the degree of ionization and dissociation of all relevant species and the equations of radiative transport. Due to the many uncertainties involved, as well as to the numerical difficulties in following the evolution of an H II region with an Eulerian grid, we have adopted the following approximate procedure for calculating T/μ .

The calculated region of space is divided into three topological regions: (a) a molecular cloud, (b) the intercloud medium, and (c) an H II region. The boundaries between the regions are assumed to be contact discontinuities. Initially the molecular cloud is centered at the origin and is separated from the intercloud medium by a cylindrical surface across which pressure equilibrium holds. An early-type star is placed in the cloud on the symmetry axis, and the initial boundary of its H II region is calculated under the assumption that the gas is at rest. As the calculation proceeds, new boundaries for the three regions are determined, and in each region the value of T/μ is set to a time-independent constant value as given in Table 1. For example, the intercloud medium has $T/\mu = 5000$, which is consistent with a neutral H gas at 5000 K but which also could result from a partially ionized gas ($\mu < 1$) at a somewhat lower temperature. The initial particle densities n_0 in each region are also listed in Table 1. The results for the champagne flow should not be significantly different if a very hot tenuous gas with $T/\mu \geq 10^6$ K is used for the intercloud medium, as long as pressure equilibrium across the cloud boundary is assumed initially. As shown in Paper I, the effect depends primarily on the pressure

TABLE 1
REGIONS OF THE CALCULATION

Material	State of Gas	$T(k)$	T/μ	n_0 (cm $^{-3}$)
Molecular cloud	H $_2$	10	5	10 3
Intercloud	H 0	5000	5000	1
Ionized gas	H $^+$ + e $^-$	8100	16200	10 3

gradient set up when the ionization front reaches this boundary.

During the course of the evolution, the motion of the surface separating the cool molecular cloud material from the hot intercloud medium was followed by the use of Lagrangian “tracers” which moved freely with the local gas velocity. It is possible to consider rather complicated surface topologies with this method—for instance, an arbitrary number (limited only by the number of grid cells available) of separated dense globules and molecular clouds embedded in the intercloud gas could be treated.

In the H II region we have assumed that a dust component is frozen into the gas and competes with it for hydrogen-ionizing photons. The additional opacity due to the dust is taken to be $\kappa_{uv} = 200 \text{ cm}^2 \text{ g}^{-1}$. For determination of the location of the boundary of the H II region as a function of time, the equation of transfer of ionizing radiation is solved under three simplifying assumptions:

1) All photons come radially from the ionizing source. Thus scattering by dust grains was not considered. Furthermore, we assumed the “on the spot” approximation.

2) Ionization equilibrium holds at all times. To a good approximation, this assumption is valid throughout most of the H II region except within the *I* front (but this zone of the flow is geometrically too thin to be properly resolved by our hydrodynamic grid).

3) The gas inside the H II region is fully ionized ($x = 1$) from the star out to the boundary where x discontinuously drops to zero. Again this assumption is valid everywhere except in the (unresolved) *I* front and during early evolutionary phases.

With the ionizing source on the axis of symmetry, the flux F of ionizing photons can be written as a function of two spatial variables $F(r, \theta)$, where r is the radial distance from the star and θ is the angle between the photon direction and the axis of symmetry. Assumption (1) allowed us to treat independently the transfer of radiation along each radial line of sight. Thus we have a system of first degree differential equations, parametrized by the angle θ :

$$\frac{\partial}{\partial r} (Fr^2) + \frac{\beta \rho^2 r^2}{\mu^2 m_{\text{H}}^2} + \kappa_{uv} \rho (Fr^2) = 0, \quad (4)$$

with the boundary condition

$$(Fr^2)_{\text{star}} = \frac{L_{uv}}{4\pi}, \quad (5)$$

where we have incorporated assumptions (1)–(3). Here L_{uv} is the total ionizing luminosity emitted by the star in all directions (7.6×10^{48} photons s^{-1}), $(Fr^2)_{\text{star}}$ is the luminosity (photons s^{-1}) emitted in any given direction θ , m_{H} is the mass of the hydrogen atom, and β the recombination coefficient ($= 3 \times 10^{-10} T_{\text{H II}}^{-3/4}$, $T_{\text{H II}} = 8100 \text{ K}$). The solution of equation (4) determines the extent of the ionized region $R_{\text{H II}}(\theta)$ for which F becomes equal to zero. We used 48 different lines of sight between $\theta = 0^\circ$ and $\theta = 180^\circ$ to accurately define the H II region boundary. At the boundary,

T/μ is allowed to vary smoothly between its values inside and outside the H II region through a narrow region with a thickness of 10% of the radial extent of the H II region.

In order to test our assumptions and the accuracy of the code, we compared the results obtained for an assumed spherically expanding H II region in a cloud of initially uniform density (Fig. 1, *solid line*) with the results of a more detailed 1-D spherically symmetric calculation. The 1-D code (described by Tenorio-Tagle 1976) is able to resolve properly the *I* front by solving the time-dependent energy, ionization balance, and radiation transport equations simultaneously with the hydrodynamics. Figure 1 (*dashed line*) shows the 1-D normalized evolution obtained for the formation and expansion phases of an H II region. The results are normalized with respect to the initial Strömgen radius (R_s) and the time at which R_s is reached by the *I* front. Results of a second run, with initial conditions identical to those used by the 2-D code (i.e., at $t = 0$, $R_{\text{I front}} = R_s$, the initial values of x and of F throughout the mesh were worked out assuming ionization equilibrium; the gas velocity u was set equal to zero throughout, etc.) are also shown (Fig. 1, *crosses*). The agreement implies that the 2-D axisymmetric code does indeed produce the correct picture of the overall H II region evolution. One should, however, be aware of the lack of detailed resolution which has not allowed us to calculate the structure of the *I* front or any temperature variation within the flow. Therefore calculations of line profiles, for example, become rather meaningless. Other important consequences of our approximate treatment for the state of the gas are: (i) All shock fronts appearing in the flow are isothermal, except when they cross a contact discontinuity surface. (ii) The possible phase transition of hot intercloud material into cool molecular gas (see Biermann

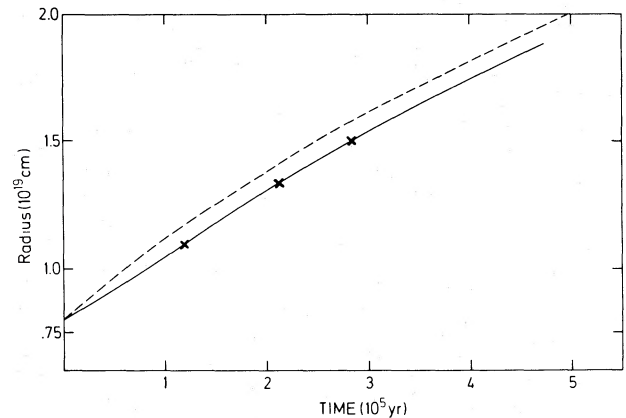


FIG. 1.—The radius of an H II region, starting initially in a constant-density cloud with $\rho = 1.67 \times 10^{-22} \text{ g cm}^{-3}$, is plotted against time. *Solid line*, calculation performed with the 2-D hydrodynamic code. *Dashed line*, a detailed 1-D calculation that includes the initial expansion of the H II region to its Strömgen radius. *Crosses*, a detailed 1-D calculation starting with the same initial condition used in the 2-D calculation, namely with the gas at rest and with the H II region at its initial Strömgen radius.

TABLE 2
PARAMETERS FOR FIGURE 2

Model	Age (yr)	m (g cm^{-3})	M (g cm^{-3})	$\Delta \log \rho$	V_{\max} (km s^{-1})
a.....	9.50×10^3	4
b.....	4.13×10^4	30
c.....	8.97×10^4	33
d.....	1.60×10^5	36.6
e.....	2.85×10^5	30
f.....	5.67×10^5	30
g.....	9.50×10^3	$10^{-23.5}$	10^{-21}	0.5	10
h.....	8.97×10^4	10^{-23}	$10^{-20.5}$	0.5	36.6
i.....	2.85×10^5	$10^{-22.5}$	$10^{-20.5}$	0.5	21.6

et al. 1972) due to the passage of a compression or a shock wave was not allowed in our treatment. Similarly, a phase transition of cool molecular material into a hot atomic gas could not be properly treated. (iii) The increase in temperature within the molecular cloud due to the close proximity of a newly born star (Yorke 1977) and within the H II region due to the hardening of the UV radiation (Hjellming 1966) was not included in the calculations.

III. RESULTS

As pointed out earlier, the champagne phase will take place as soon as the density discontinuity (between cloud and IC) becomes ionized. Therefore, the amount of cloud material that surrounds a newly formed star determines the time at which this phase will occur. In principle, depending on how deep in the cloud the star is born, it could happen during either the formation or the expansion phase. The *I* front, just before it crosses the discontinuity, would be of *R* or *D* type, respectively, and in the latter case will be preceded by a shock wave. The detailed ionization of the density gradient and the resulting flow in both cases have been described in Paper I. Here we present the results of the 2-D calculations which give a more complete evolutionary picture. After describing the flows produced in the *R* and *D* cases (cases 1 and 2) we discuss two additional cases (3 and 4) involving champagne flows which are of observational interest.

In all cases we have assumed that an early type star ($T_{\text{eff}} \approx 4 \times 10^4$ K) is placed on the symmetry axis (the *Z*-axis) of a cylindrical cloud which is in pressure balance with the undisturbed IC medium (see Table 1). In order to present a clear view of the overall flow, for each case we show a time sequence of cross-sectional views through the axis of symmetry, showing either the entire computational grid or a detailed portion of the flow. Each figure is accompanied by a table (Tables 2–5) which gives the evolutionary time, maximum (*M*) and minimum (*m*) density, density contour interval,

TABLE 3
PARAMETERS FOR FIGURE 3

Model	Age (yr)	m (g cm^{-3})	M (g cm^{-3})	$\Delta \log \rho$	V_{\max} (km s^{-1})
a.....	2.56×10^4	$10^{-23.5}$	10^{-21}	0.5	7.2
b.....	5.04×10^4	$10^{-23.5}$	$10^{-20.5}$	0.5	9.0
c.....	7.58×10^4	$10^{-23.5}$	$10^{-20.5}$	0.5	16.0
d.....	7.58×10^4	$10^{-23.5}$	$10^{-20.5}$	0.5	16.0
e.....	1.01×10^5	$10^{-23.5}$	$10^{-20.5}$	0.5	22.0
f.....	1.24×10^5	$10^{-23.5}$	$10^{-20.5}$	0.5	24.0

$\Delta \log \rho$, and the maximum detected velocity V_{\max} for each model presented.

a) Case 1

The exciting star, embedded in a dusty cloud medium, produces an initial Strömgren sphere with a radius $R_s = 1.53 \times 10^{18}$ cm. We placed the star at a distance $Z = 7.88 \times 10^{18}$ cm from the center of the cloud and the edge of the cloud at $Z = 9.5 \times 10^{18}$ cm. Thus the *I* front is about to break through the edge of the cloud in the *Z*-direction. After a very short time an *R* type *I* front moves into the IC medium and establishes a large pressure gradient at the density discontinuity ($\Delta \log P = 3$). Figure 2a shows the full grid at a time $t = 9.5 \times 10^3$ yr. The boundary of the H II region is roughly spherical inside the cloud, but in the IC medium it forms a thin conical region of length much larger than the dimensions of the grid. The spherical part of the H II region has just started to expand ($v \approx 4 \text{ km s}^{-1}$) while the ionized material at the edge of the cloud begins to stream away from the cloud with a larger velocity ($v \approx 10 \text{ km s}^{-1}$). An isothermal shock forms and accelerates into the ionized IC medium. Figure 2g is an enlarged picture of the flow at this time which shows the deformation of the (initially straight) density contours. The calculated cloud “boundary” follows the shock into the IC medium; since its motion is calculated from velocities slightly behind the actual cloud edge, at this moment it is moving somewhat more slowly than the edge of the disturbance.

TABLE 4
PARAMETERS FOR FIGURE 4

Model	Age (yr)	m (g cm^{-3})	M (g cm^{-3})	$\Delta \log \rho$	V_{\max} (km s^{-1})
a.....	8.02×10^3	$10^{-23.5}$	10^{-21}	0.5	5.5
b.....	3.1×10^4	$10^{-23.5}$	$10^{-20.5}$	0.5	15.3
c.....	7.02×10^4	10^{-24}	$10^{-20.5}$	0.5	38.0
d.....	1.03×10^5	10^{-23}	$10^{-20.5}$	0.5	40.0

FIG. 2.—The evolution of case 1, shown in the (*X*, *Z*)-plane, where the *Z*-axis is the symmetry axis. *Dashed-dot line*, the boundary of the ionized region. *Crosses*, boundary of the material that was originally in the molecular cloud. *Solid*, alternating with *dashed lines*, equidensity contours, with *m* and *M* the contours corresponding respectively to the minimum and maximum densities shown. *Triangle*, the location of the exciting star. *Solid arrows*, velocity vectors with length proportional to speed. The scale for the velocity is given in the lower right-hand corner of each plot. For further details, see Table 2.

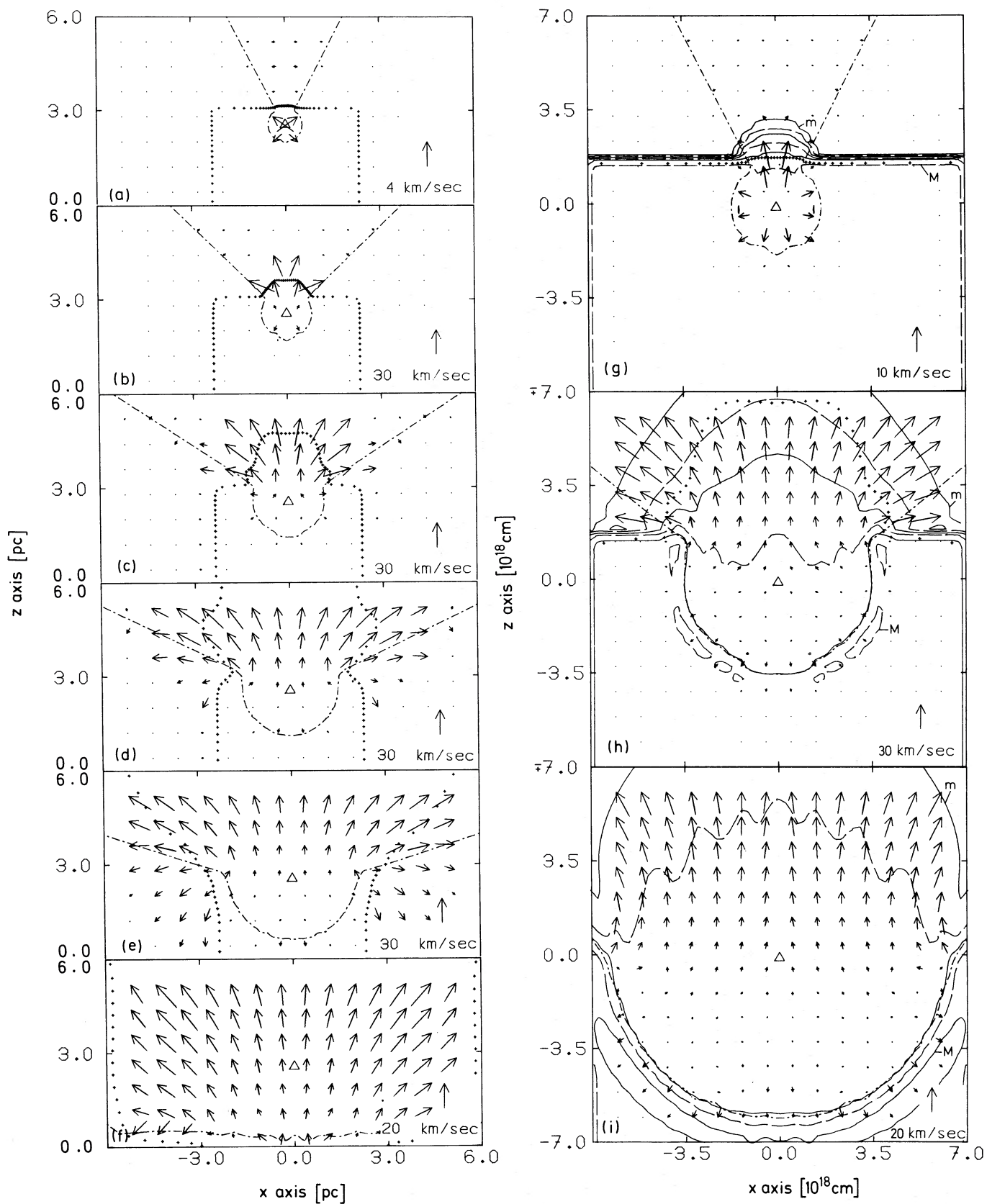


FIG. 2

TABLE 5
PARAMETERS FOR FIGURE 5

Model	Age (yr)	m (g cm^{-3})	M (g cm^{-3})	$\Delta \log \rho$	V_{max} (km s^{-1})
a.....	2.56×10^4	8.4
b.....	3.59×10^4	8.7
c.....	6.67×10^4	36.0
d.....	8.44×10^4	38.0
e.....	1.0×10^5	36.8
f.....	1.16×10^5	36.8
g.....	3.59×10^4	$10^{-23.5}$	$10^{-20.5}$	0.5	25.3
h.....	8.44×10^4	$10^{-23.5}$	$10^{-20.5}$	0.5	36
i.....	1.16×10^5	$10^{-22.5}$	$10^{-20.5}$	0.5	30

Figures 2*b* and 2*c* show the more developed and accelerated champagne flow being driven into an increasingly wider cone of IC ionized matter. An enlargement of the flow at $t = 8.97 \times 10^4$ yr (see Fig. 2*h*) shows material that was originally part of the cloud moving just behind the shock into the IC medium at about the shock velocity which has now increased to about 36 km s^{-1} . The density maximum in the flow occurs in the shocked cloud material just ahead of the *D* type front that is still progressing through the cloud. One can also see the effects of a well-developed rarefaction wave moving through the ionized cloud material from the cloud boundary toward the star, causing the outward acceleration of the rarefied matter. This effect, along with the increasing extent of the ionized surface of the cloud, results in a primary flow perpendicular to that surface. Pressure gradients in the *X*-direction result in a secondary almost spherical flow that fills up the volume of the cone. At this time the pressure difference between the conical H II region and the surrounding neutral IC material also results in flow of gas into that material; the velocities in the neutral gas increase to 30 km s^{-1} at later times.

As the evolution continues, the expansion of the spherical portion of the H II region in the *X*-direction begins to affect the lateral surface of the cloud. Figures 2*d* and 2*e* show the nature of the flow at the time when the "corner" of the cloud begins to be ionized. It is only after this time that an H II region associated with a cloud will begin to show its ionizing source when observed edge-on. An enlargement of the spherical part of the H II region (Fig. 2*i*, taken at the same time as Fig. 2*e*) shows the well-defined density maximum ahead of the inward-moving *I* front as well as the rarefaction wave that has now progressed from the cloud boundary inward to a point interior to the star. Thus material in the inner part of the H II region, which originally was expanding away from the star in the negative *Z*-direction, is now affected by the champagne flow and is beginning to move outward toward the cloud boundary.

A final view of the evolution (Fig. 2*f*) shows the star separated by some 3 pc from the edge of a nearly flat, dense cloud, embedded in lower-density ($\rho \sim 7 \times 10^{-23} \text{ g cm}^{-3}$) material that continues to stream away from the cloud. The velocity of outflow increases from roughly 10 to 30 km s^{-1} as one proceeds outward from

the cloud's edge. It is important to note that cloud material that initially was interior to the star has now been blown past it, resulting in a reduction in the density in that region. Thus an increasingly larger supply of photons reaches the inward-moving *I* front and speeds up the evaporation of the cloud. A more detailed solution of this problem will be presented in a later communication. The total amount of material evaporated during the evolution was about $1000 M_{\odot}$, implying a rate of $2 \times 10^{-3} M_{\odot} \text{ yr}^{-1}$. At the end of the calculation the distance from the star to the champagne shock (now well outside the computational grid) was of the order of 20 pc.

b) Case 2

The initial parameters in this case were selected in such a way that the H II region could expand for some time ($\sim 80 \times 10^3$ yr) into the (constant density) cloud before meeting the density discontinuity. For such an effect to occur, the star was placed at a distance of $2.26 \times 10^{18} \text{ cm}$ from the edge of the cloud, whose height and radius were $2.4 \times 10^{19} \text{ cm}$ and $1.2 \times 10^{19} \text{ cm}$, respectively. The main features of the expansion are clearly shown in Figures 3*a*, 3*b*, and 3*c*. As the ionized gas at the edge of the H II region begins to expand, a rarefaction wave forms and begins to move toward the central source. The rarefaction wave (traveling with the speed of sound) will eventually produce a shell of lower density material that has been accelerated outward. Thus the maximum density of the nebula in Figure 3*a* can be found at the exciting star while a local minimum occurs just inside the edge of the ionized region. As the expansion continues and the rarefaction wave moves closer to the star (see Fig. 3*b*), a new density maximum appears in the surrounding neutral gas. This is due to the passage of a shock wave (predicted by Kahn 1954) that appears in the flow in order to modify and set the required upstream conditions for the propagation of a *D* type *I* front. In Figure 3*c* one can see the effect on the flow produced after the rarefaction wave has bounced out from the center of symmetry of the spherical nebula. The newly rarefied gas now begins to move toward the star, while the whole ionized region continues expanding with a velocity of the order of the sound speed ($u_{\text{ex}} \lesssim 10 \text{ km s}^{-1}$). At all times the rarefaction of the H II region allows the *I* front to sweep up new material. In this way the *I* front acts like a piston on the outer shock that produces the density maximum.

The evolution so far is what one would expect from the classical expansion theory; this phase continues until the outer shock intersects with the density gradient. The effects produced during the interaction are shown in Figure 3*d* which is taken at the same time as Figure 3*c* but with a shifted origin. As the outward shock crosses the discontinuity, the neutral gas receives a kick that produces the deformation of the density contours at the cloud's edge. A shock wave passing through a medium of decreasing density will speed up initially, but eventually this will cause its decay, as the driving piston (the *I* front) is left behind and the sound

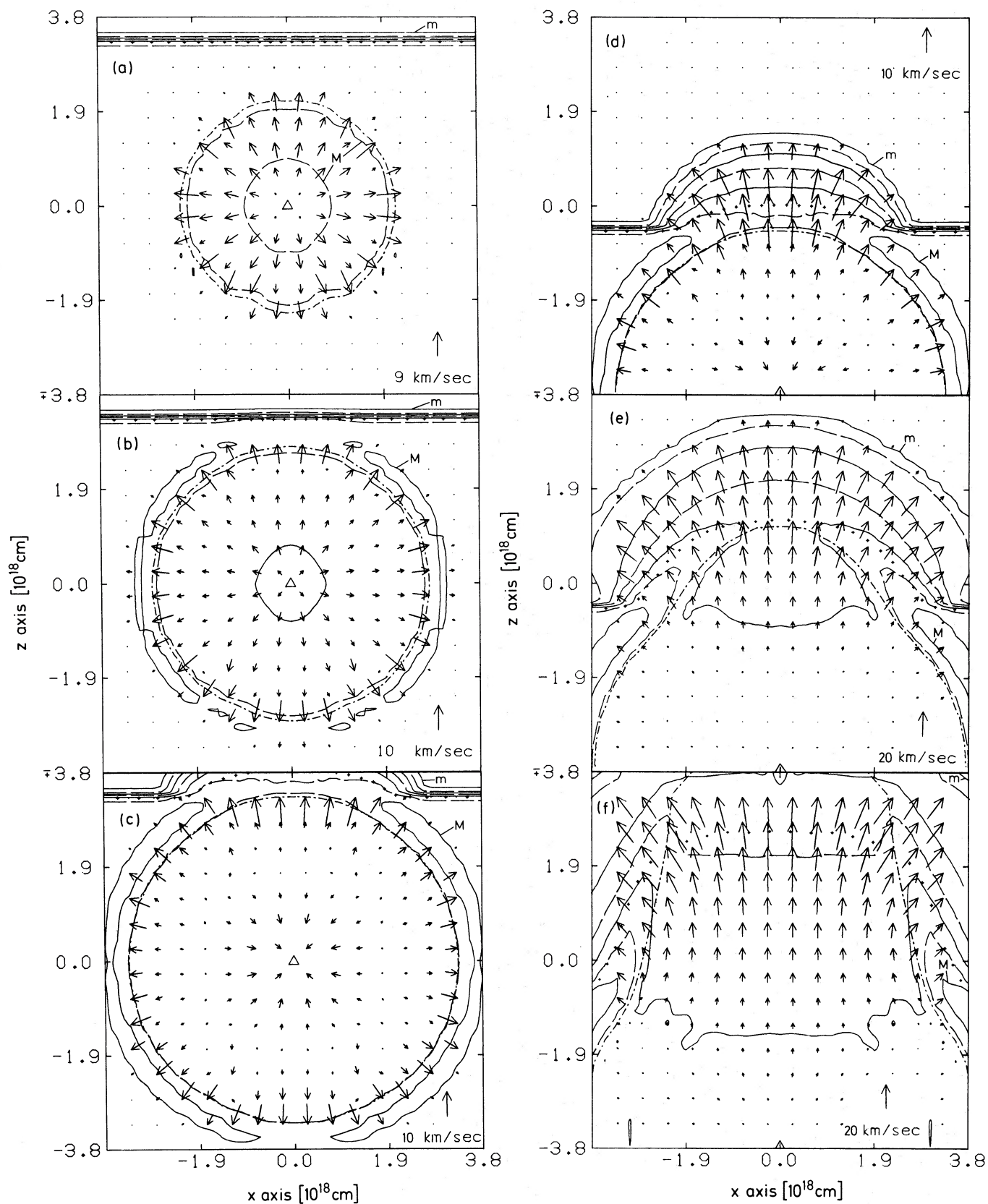


FIG. 3.—The evolution of case 2. Symbols have the same meaning as in Fig. 2. For further details, see Table 3.

speed c in the hot IC medium weakens the disturbance (as $\text{Mach} = U_{\text{shock}}/c$). The D type I front continues working its way out into the shocked gas, catching up first with the expanding cloud material (Fig. 3e) and later with the leading disturbance. The I front then becomes supersonic and rushes through the IC medium (Fig. 3f), creating a large pressure gradient that eventually develops into a champagne flow. Large outward velocities ($u \gtrsim 30 \text{ km s}^{-1}$) can now be detected. The “cone” shaped H II region in the intercloud medium together with the refraction wave that moves into the ionized cloud have also appeared. Thus, the flow begins to resemble the solution of case 1.

The calculation was rerun including the cloud's self-gravity; however, the results were practically identical to those shown in Figure 3. The free-fall time of the cloud is 1.6×10^6 years while the time for the expanding H II region to reach the edge of the cloud is about 7.5×10^4 years. During this time gravity can affect the cloud structure only slightly. Also the escape velocity from the $2000 M_{\odot}$ cloud is only 2.7 km s^{-1} while the flow velocities range from 10 to more than 30 km s^{-1} .

c) Case 3

The star, placed at the origin of the grid, is located at the center of a thin cylindrical cloud with a radius of 2.6 pc (equal to the size of the grid in the X -direction) and with a total thickness of 1.31 pc. Thus the outer edge of the initial H II region (radius 0.5 pc) is 0.16 pc inside the cloud edge, a distance across which it travels in 1.6×10^4 yr. The sequence of pictures in Figure 4 shows the entire computational grid. Figure 4a shows the early stages of the expanding H II region. At 3.1×10^4 yr the H II region has broken through the edge of the cloud simultaneously in both directions and has produced the double cone structure illustrated in Figure 4b. The isothermal shock at this time is propagating into the IC medium behind the I front, and the physical situation is similar to that in the early stages of case 1. The angle of the cone continues to widen and material pours out of the cloud (Figs. 4c, 4d). By 7×10^4 yr (Fig. 4c) the refraction wave has reached the center, the density increases outward from the star out to a distance of about 0.3 pc, and material in this region flows toward the star. The density at the star has been reduced to $2.8 \times 10^{-22} \text{ g cm}^{-3}$. At 1.03×10^5 yr (Fig. 4d) note that as the ionized region works its way laterally into the cloud, the newly ionized material quickly joins the main flow in the $\pm Z$ -direction. At this time the density at the star has again slightly increased; the mean density in the “evacuated” region is about $4 \times 10^{-22} \text{ g cm}^{-3}$. Thus about $250 M_{\odot}$ has been expelled in 10^5 yr, a rate of $2.5 \times 10^{-3} M_{\odot} \text{ yr}^{-1}$, a figure very similar to that derived in case 1, even though the geometry is quite different. In the expanding material outside the initial cloud the velocities increase from 10 to more than 30 km s^{-1} , and the corresponding densities decrease from 2.4×10^{-22} to $3.3 \times 10^{-23} \text{ g cm}^{-3}$. Note that the escape velocity of the ($\sim 10^3 M_{\odot}$) cloud is of the

order of 4 km s^{-1} ; thus we expect the entire cloud to be disrupted. Its self-gravity, if included, would not play an important role.

d) Case 4

The cylindrical cloud of radius $r = 2$ pc and height $h = 2r$ contains a star located on the symmetry axis at a distance 0.7 pc from the surface of the cloud. At the standard density of $1.67 \times 10^{-21} \text{ g cm}^{-3}$ the cloud contains $1.13 \times 10^3 M_{\odot}$. The initial H II region, which does not contain dust in this particular case, extends to a radius of 0.57 pc from the star, rather than the 0.5 pc obtained in cases 1, 2, and 3. A small spherical globule with a radius of 0.46 pc is placed with its center on the symmetry axis 0.66 pc outside the cloud. The density and temperature in the globule are the same as in the cloud, and its mass is $9.6 M_{\odot}$ while the Jeans mass is $11.6 M_{\odot}$. The motion of the boundary of the globule is followed by the method of Lagrangian tracers described in § II, and the temperature inside the boundary is constant with time at 10 K. Initially the globule is in pressure equilibrium with the surrounding IC medium.

The configuration at an early time is shown in Figure 5a. The H II region is symmetrically expanding; the champagne flow has just started to break out of the edge of the cloud and to meet the obstacle of the globule. The I front moves through the globule at a velocity of about 8 km s^{-1} , compressing the material ahead of it. By 3.6×10^4 years, photons are able to escape (Fig. 5b) readily through the low-density material on the side of the globule, creating an H II region in the form of a conical shell that gradually broadens and increases in vertex angle. In the conical shell an R type I front moves rapidly through the IC gas while D type fronts proceed through the cloud and the globule. Details of the flow at this time are shown in Figure 5g. The H II region in the outer zone beyond the globule has a somewhat higher pressure than the surrounding neutral gas, and the pressure gradient produces motion of material into the exterior IC neutral gas and into the “shadow” region behind the globule. Note that the diffuse radiation from the H II region would ordinarily produce some ionization in the “shadow”; this effect is not taken into account in the calculations.

As the evolution (Figs. 5c, 5d) progresses, the globule is becoming noticeably flattened as the I front eats into it. The calculated globule “boundary” moves inward with the I front; globule material behind the I front is evaporated and begins to flow back toward the cloud, where it interacts with the champagne flow, producing a slight density maximum in the region between cloud and globule. The velocities of flow past the globule increase to more than 30 km s^{-1} , and significant flow of material occurs into the “shadow” zone (cf. Fig. 5h). At about 8×10^4 years, a refraction wave reaches the exciting star, and in the region within 0.5 pc of the central source the gas flows toward it at velocities of $\sim 3 \text{ km s}^{-1}$.

During the later phases of the evolution (Figs. 5e, 5f) rapid gas flow past the globule continues and

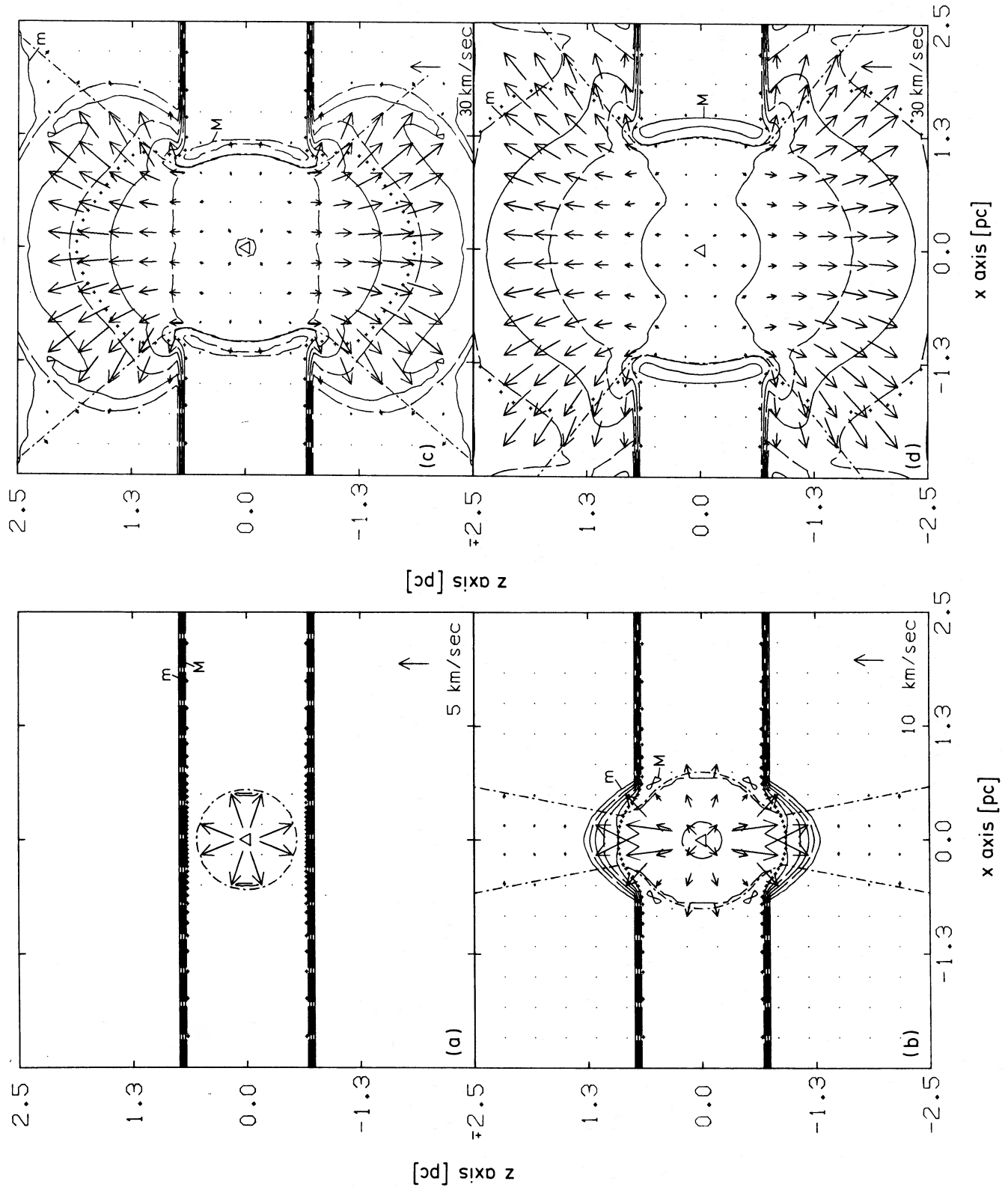


FIG. 4.—The evolution of case 3. Symbols have the same meaning as in Fig. 2. For further details, see Table 4.

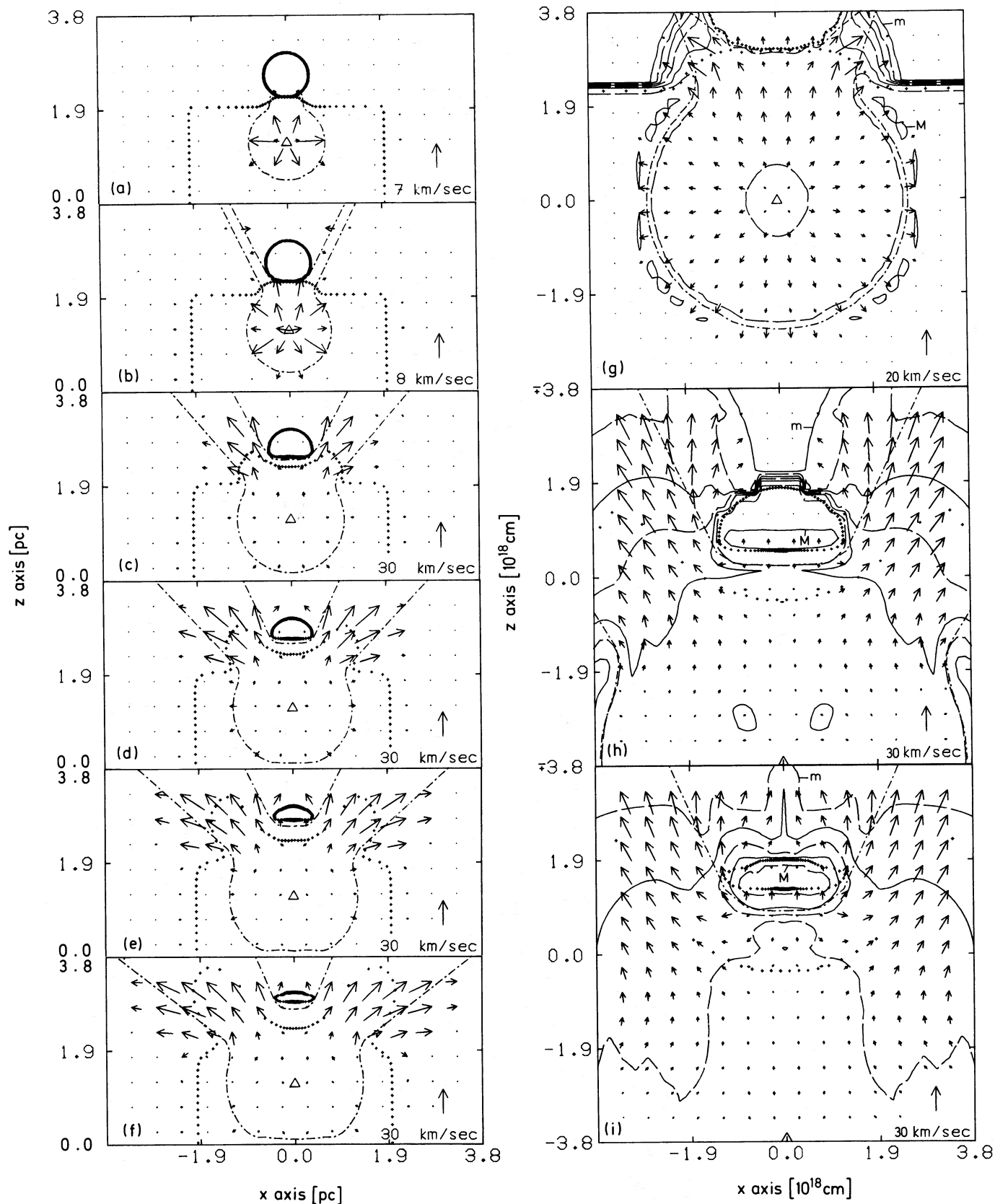


FIG. 5.—The evolution of case 4. Symbols have the same meaning as in Fig. 2. In addition, the globule boundary is indicated by crosses. For further details, see Table 5.

includes the entire region behind the globule, where a "wake" forms. The number of grid points is not sufficient to resolve the details of this flow. Outward flow from the front surface of the globule is evident in Figure 5*i*; this evaporated material joins the main flow past the globule. The H II region itself continues to expand into the cloud, exhibiting similar effects to those described in case 2. At the end of the calculation the globule itself has been compressed by about a factor of 3.5 over its initial density; thus its Jeans mass has decreased to $6 M_{\odot}$. At its original mass the entire globule would now be unstable and could gravitationally collapse to form a star. However, the situation is complicated by the fact that the globule has lost an estimated 30% of its mass by evaporation. The remaining $7 M_{\odot}$ is barely Jeans-unstable. The numerical resolution at the end of the calculation is insufficient to determine the mass and density of the globule accurately. Further calculations will be necessary to determine whether part or all of the globule will actually begin to collapse.

IV. COMMENTS AND CONCLUSIONS

From the calculations here presented, one becomes aware of the importance of the new phase proposed in Paper I for the evolution of H II regions. The two more general cases (cases 1 and 2) and some interesting applications (cases 3 and 4) have been fully described in the preceding section. Here we mention other important consequences of our models, particularly in connection with the observations of ionized regions in space.

One can first of all conclude that the champagne phase gives a clear explanation for the observed association between dense clouds and ionized nebulae. The phenotypical resemblance between our models and observed structures is indeed striking. For example, a comparison between the models of case 4 (Fig. 5) and the well-resolved flat compressed globules immersed in M16 (see Spitzer 1968, frontispiece) is encouraging. We can also compare cases 1 and 2 (Figs. 2 and 3) with objects like S157, S158 (for optical and radio maps of these regions, see Israel, Habing, and de Jong 1973) or with NGC 2024 or M17, etc.; in these regions the ionizing stars are still hidden from us behind the lateral edges of the dark clouds where they formed. Thus optically we only see the champagne flow being driven out of the cloud, while in the radio continuum another strong component (s) is present.

Our models would resemble other nebulae (like Orion) if one looked at them from a direction that would allow one to see the star(s). For the particular case of Orion, we can conclude that the rarefaction wave produced after the ionization of the discontinuity has gone past the stars (see Figs. 2*e*, 2*f*), resulting in the outward motion of the formerly inward-moving gas. In this way (with the present model) one can understand the observed [O II] being redshifted with respect to [O III] (Wilson *et al.* 1959) and the [Fe II] redshifted with respect to [O II] found

by Kaler (1967) when looking at the central parts of the nebula. We know that ions with low ionization potential originate close to the H II–H I boundary and [O III] is only produced in the neighborhood of the star. Thus the head of the rarefaction wave must have already crossed the stars, causing the rarefaction and outward acceleration of the zone containing [O III], and perhaps beginning to decelerate the inward-moving zone where [O II] is present. Surely the rarefaction wave has not yet reached the inward-moving *I* front where [Fe II] is produced; otherwise the straightforward evaporation of the gas would have started and all the ionized gas should be moving toward us (see Zuckerman 1973, 1975). Our present picture could be improved upon if we considered more ionizing sources in the vicinity of our star and their consequent champagne flows. With the present model, if an observer scans along a line that crosses the position of the star, he should not expect to see a maximum velocity (*u*) of approach (or recession) near the star. Nor should the velocity along the line of sight decrease in magnitude as he moves away from the source. This is in contradiction with the expectations of the "classical" theory and in agreement with the observations (see Osterbrock 1974).

In the light of the expansion theory of H II regions the energy balance is thought to be as follows: The UV radiation from the star causes ionization and heating of the surrounding gas. The average energy of a photoejected electron is kT_* (where k is the Boltzmann constant and T_* is the surface temperature of the star; see Kahn and Dyson 1965), and $\psi_i + kT_*$ is the average UV photon energy, where $\psi_i = 13.6$ eV. Thus only a small fraction of the total stellar energy [$\Gamma = kT_*/(\psi_i + kT_*)$] is converted into heat (for $T_* \approx 40 \times 10^3$ K, Γ becomes of the order of 20%). Energy escapes the ionized nebula via recombination, and a good fraction of Γ is also lost as the gas cools down to its equilibrium temperature. Thus only a very small fraction of the total energy can be converted into mass motions. Our calculations have shown how the ionization of a density discontinuity (from the inside) can be a very important source of kinetic energy for the ionized gas, changing appreciably the results of the classical theory. If one compares the thermal to the kinetic energy of the ionized gas that is undergoing the champagne phase, the ratio $P/[\rho(\gamma - 1)]/(0.5u^2)$ becomes $\lesssim 1$ (instead of 10^{2-3} or larger). Thus if an early type star radiates L_{UV} UV photons s^{-1} during its lifetime t_f , it will produce a total amount of kinetic energy in the surrounding gas which is of the order of $fkT_*t_fL_{UV}$, where f represents a correction factor that accounts for the fraction of the energy that remains as heat and the energy that is lost by radiation. If f is about 0.1, we would expect an O star radiating 10^{49} UV photons s^{-1} to produce 5×10^{50} ergs of mechanical energy during its lifetime of 3×10^6 yr. To compare with the actual calculation, we take an approximate evaporation rate of $3 \times 10^{-3} M_{\odot} yr^{-1}$ and a velocity of 30 km s^{-1} for the evaporated gas. The mass of ejected material is then $9 \times 10^3 M_{\odot}$ over the lifetime of the O star. During this time a

comparable amount of intercloud gas is swept up and accelerated to this velocity; thus the total kinetic energy would be approximately 1.5×10^{50} ergs. The discrepancy can be accounted for by the photons that ionize the gas ahead of the champagne shock but do not result in mass motion during the lifetime of the O star, and by those photons that drive the *D* type front into the remnant of the molecular cloud at relatively low velocities. In any case the process we are considering results in an appreciable mechanical energy input to the interstellar medium, comparable to (although somewhat less than) that provided by the average supernova event.

The large velocities here found are a function of the pressure contrast set once the density discontinuity becomes ionized (Tenorio-Tagle and Bedijn 1978). Note that an isothermal rarefaction wave can cause matter to reach limiting velocities larger than three times sound velocity; in fact, velocities up to 40 km s^{-1} were observed (see Tables 2, 4, and 5). The larger the pressure gradient, the stronger the champagne shock and thus the larger u becomes. These large velocities imply a fast growth of the radius of H II regions (note that we are referring only to the density-bounded side of the region, through which a large fraction of ionizing photons leak)—faster than that predicted by the expansion theory (where $u_{\text{gas}} \lesssim 10 \text{ km s}^{-1}$). Therefore, the calculated age of expansion becomes at least a factor of 3 smaller. The age of a nebula worked out in this way (t_{ch}) will tell us for how long the nebula has undergone the champagne phase, but it would say nothing about its real age. This depends only on the age of the exciting star (t_s). By working out the difference $t_a = t_s - t_{\text{ch}}$ and applying the classical

expansion theory, namely,

$$R_d = \left(1 + \frac{7}{4} \frac{c_i t}{R_s}\right)^{4/7} R_s,$$

where c_i is the isothermal sound speed (Spitzer 1968), one could find (using $t = t_a$) a lower limit for R_d which represents how deep into the cloud the star was initially formed. (Of course, one should also have an estimate of N_{cloud} and F_* in order to estimate R_s .) In this way our model resolves the paradox of the age of the Orion Nebula (see Shaver 1976).

The question of whether or not neutral globules in H II regions can collapse to form stars has been studied under the assumption that initially the globule is in pressure equilibrium with the IC gas and detached from the cloud in which a hot star and its H II region originate. The globule becomes aware of the existence of the star only after the *I* front has crossed the cloud discontinuity and the champagne phase begins. The globule experienced considerable compression, but also a large fraction of its initial mass becomes ionized. One can see that the champagne flow plays a main role in the evolution of the condensation, and the contribution of both gas and ram pressure of the material in the champagne flow to the condensation's external pressure (normally taken as the IC ionized gas pressure only) could result in gravitational instability in the globule. The result of our particular calculation suggests, however, that the globule must be rather close to its Jeans limit before the compression takes place, in order for star formation to occur.

Other interesting cases have now been calculated and will be described in future communications.

REFERENCES

- Biermann, P., Kippenhahn, R., Tscharnuter, W., and Yorke, H. 1972, *Astr. Ap.*, **19**, 113.
 Black, D. C., and Bodenheimer, P. 1975, *Ap. J.*, **199**, 619.
 Hjellming, R. M. 1966, *Ap. J.*, **143**, 420.
 Israel, F. P., Habing, H. J., and de Jong, T. 1973, *Astr. Ap.*, **27**, 143.
 Kahn, F. D. 1954, *B.A.N.*, **12**, 187.
 Kahn, F. D., and Dyson, J. E. 1965, *Ann. Rev. Astr. Ap.*, **3**, 47.
 Kaler, J. B. 1967, *Ap. J.*, **148**, 925.
 Mansfield, V. N. 1972, Ph.D. thesis, Cornell University.
 Mathews, W. G., and O'Dell, C. R. 1969, *Ann. Rev. Astr. Ap.*, **7**, 67.
 Osterbrock, D. E. 1974, *Astrophysics of Gaseous Nebulae* (San Francisco: Freeman), chap. 6.
 Shaver, P. A. 1976, in *Topics in Interstellar Matter*, ed. H. von Woerden (Dordrecht: Reidel), p. 49.
 Spitzer, L., Jr. 1968, *Diffuse Matter in Space* (New York-London-Toronto: Interscience), p. 192.
 Tenorio-Tagle, G. 1976, *Astr. Ap.*, **53**, 411.
 ———. 1979, *Astr. Ap.*, **71**, 59 (Paper I).
 Tenorio-Tagle, G., and Bedijn, P. 1978, *Astr. Ap.*, submitted.
 Terzian, Y., and Balick, B. 1974, *Fundamentals of Cosmic Physics*, Vol. 1, No. 4, p. 301.
 Wilson, O. C., Münch, G., Flather, E. M., and Coffeen, M. F. 1959, *Ap. J. Suppl.*, **4**, 199.
 Yorke, H. W. 1977, in *IAU Colloquium No. 42*, ed. R. Kippenhahn, J. Rahe, and W. Strohmeier (*Veröffentlichungen der Remis-Sternwarte Bamberg*, Vol. **11**, Nr. 121), 38.
 Zuckerman, B. 1973, *Ap. J.*, **183**, 863.
 ———. 1975, *H II Regions and Related Topics*, ed. T. L. Wilson and D. Downes (*Lecture Notes in Physics*, Vol. **42**) (Berlin-Heidelberg-New York: Springer-Verlag), p. 360.

PETER BODENHEIMER: Lick Observatory, University of California, Santa Cruz, CA 95064

GUILLERMO TENORIO-TAGLE: ESO/CERN, CH-1211 Genève, Switzerland

HAROLD W. YORKE: Universitäts-Sternwarte Göttingen, Geismarlandstrasse 11, D-3400 Göttingen, Federal Republic of Germany